# Electric Field Confinement and Enhancement in a Silver Film Fabry−Pérot Interferometer†

**Feng Yu, Haining Wang, and Shengli Zou***

*Department of Chemistry, University of Central Florida, 4000 Central Florida Boulevard, Orlando, Florida 32816-2366*

*Received: December 7, 2008; Revised Manuscript Received: January 30, 2009*

Using the discrete dipole approximation method and exact analytical solutions, we demonstrate that an incident electromagnetic wave can be confined and enhanced between two silver layers due to the Fabry−Pérot effect. The enhanced electric field between the two layers depends on the distance between the two layers and each layer's thickness. An enhanced electric field, $|E|^2$, with an enhancement factor of 50 was obtained at distances 100 nm above the surface. The resonance wavelength increases linearly with the distance between the two layers and varies with their thicknesses. Reduced scattering and enhanced absorption efficiencies of the interferometer at resonance wavelength were observed. The effect demonstrated here could be applied for studying both enhanced fluorescence and nanolasers.

## Introduction

A standard Fabry−Pérot (FP) interferometer[1] is composed of a transparent plate with two parallel, highly reflecting mirrors on each side. High-resolution spectra can be obtained with the FP interferometer[2,3] due to multiple reflections of the electromagnetic wave between the mirrors. The FP interferometer has been utilized in different applications, such as optical sensors,[4−8] waveguides,[9−12] and lasers.[13−18]

Using two thin silver layers as mirrors, we demonstrate that the electric fields between the two parallel layers can be significantly enhanced. The magnified electric field could be useful in enhanced fluorescence studies.[19−27] The enhanced local electric field near metal nanoparticles[28−32] has been investigated both theoretically and experimentally. The local enhancement is due to the excitation of surface plasmons, which are collective excitations of conduction electrons of the metal nanoparticles. The enhanced local electric field has been utilized in surface enhanced Raman scattering[32−39] and fluorescence studies.[19−27] Compared with the enhancement factor of $10^{14}$ found in surface enhanced Raman scattering,[37] the enhanced fluorescence signal could be amplified only by a moderate factor of 10-fold.[40] The fluorescence signal enhancement is limited by the quenching effect of the metal surface to nearby fluorophores or quantum dots at emission frequency.[19,25,41−46] Therefore, enhanced electric fields generated far away from the metal surface, where the quenching effects can be minimized, may lead to amplified fluorescence signals.

The effect can also be applied in nanolaser studies.[13−17] Yoshida et al.[13] demonstrated a 342 nm multiple quantum well laser using a layered structure. A surface-plasmon-assisted semiconductor laser was reported by Yu et al.[14] Manolatou et al.[17] utilized the confined surface plasmon mode to pump and shape the output in semiconductor materials. In this manuscript, we demonstrate that an enhanced electric field, $|E|^2$, of 50 can be achieved over 100 nm away from the film surface. This enhancement is due to the Fabry−Pérot interference effect. For quantum dots or semiconductor materials placed in the enhanced electric field region, which is over 100 nm away from the metal surface, enhancements from both excitation and emission frequencies are possible. Additionally, an improved enhancement factor can be expected, since the quenching effect of the silver metal to the quantum dot or semiconductor materials at the emission frequency is avoided[25] at such a long distance.

## Computational Method

The discrete dipole approximation (DDA) method[47] is a finite element method for the calculation of the optical properties of particles with arbitrary shapes. In the DDA method, the target particle is divided into an array of $N$ polarizable cubes. The interactions between the excited dipoles of all the cubes and the incident electromagnetic wave are treated with a coupled dipole approximation. The local electric field at each cube position can be obtained from the solution of $3N$ linear equations. The optical properties of the target particle can be calculated once the local electric field at each cube position is obtained. The convergence of the calculations depends on the grid length of the polarizable cube. An exact solution can be approached as the grid size becomes smaller. The computational time is proportional to the number of cubes included in the simulations. The extinction and scattering cross sections of a target with $N$ cubes can be calculated using the following equations

$$C_{\text{ext}} = \frac{4\pi k}{|E_0|^2} \sum_{j=1}^{N} \text{Im}\left(E^*_{\text{inc},j} \cdot P_j\right) \tag{1}$$

$$C_{\text{sca}} = \frac{k^4}{|E_0|^2} \int \mathrm{d}\Omega \left| \sum_{j=1}^{N} [P_j - \hat{n}(\hat{n} \cdot P_j)] \exp(-ik\hat{n} \cdot r_j) \right|^2 \tag{2}$$

where $N$ is the number of cubes of the target; $k$ represents the wave vector at incident wavelength, $\lambda$; $E_0$ is the amplitude of the incident electric field; $E_{\text{inc}}$ is the incident electric field at cube j's position; $P_{\text{j}}$ is the induced electric dipole of cube $j$; $\hat{n}$ represents the unit vector along the scattering direction; and $r_j$ refers to the coordinate vector of cube j. The absorption cross section, $C_{\text{abs}}$, is given by $C_{\text{ext}} - C_{\text{sca}}$. The extinction, scattering,

† Part of the "George C. Schatz Festschrift".

* Electronic mail: szou@mail.ucf.edu.

10.1021/jp810756e CCC: $40.75 
Published on Web 03/04/2009

and absorption efficiencies are given by the ratios of the corresponding cross sections over the physical cross sections of the film or particle. For the infinite films discussed in the manuscript, periodic boundary conditions are applied in the DDA program.[47,48]

The analytical solution of the reflectance and transmittance of a single slab can be found in pages 36−38 of Bohren and Huffman's book.[49] The scattering (reflection), absorption, and extinction spectra of the film can be obtained once its reflectance and transmittance are obtained. For a multilayer film[50] with normal incident light, the spectra of the film can also be obtained with equations satisfying the following electric and magnetic boundary conditions of all the layers in the film:

$$E_j^+ \exp(ikN_jh_j) + E_j^- \exp(-ikN_jh_j) = E_{j+1}^+ \exp(ikN_{j+1}h_{j+1}) + E_{j+1}^- \exp(-ikN_{j+1}h_{j+1}) \quad (3)$$

$$E_j^+ \exp(ikN_jh_j) - E_j^- \exp(-ikN_jh_j) = \frac{N_{j+1}}{N_j}[E_{j+1}^+ \exp(ikN_{j+1}h_{j+1}) - E_{j+1}^- \exp(-ikN_{j+1}h_{j+1})] \quad (4)$$

where $j$ refers to the $j$th boundary of the film, $h_j$ indicates the coordinate of the $j$th boundary along the wave vector direction, $N_j$ is the index of refraction of the $j$th medium, $E_j^+$ and $E_j^-$ represent the amplitudes of the electric fields for waves propagating along or opposite the incident wave direction in the $j$th medium, and $k$ denotes the wave vector of the incident wave. When the environments on both sides of the film are the same, the reflectance and transmittance of a multilayer film with $n$ boundaries can be calculated as

$$R = \left|\frac{E_1^-}{E_1^+}\right|^2, \quad T = \left|\frac{E_n^+}{E_1^+}\right|^2 \quad (5)$$

where $E_1^+$, $E_1^-$, and $E_n^+$ are the amplitudes of the incident, reflected, and transmitted waves, respectively, and $R$ and $T$ are the reflectance and transmittance of the film, respectively. The scattering efficiency of the system is the same as $R$, the extinction efficiency is given by $1 - T$, and the absorption efficiency equals $1 - T - R$. The absorption efficiency of each layer and the electric fields in the film can also be calculated once the electric field amplitudes in all the layers are obtained.

## Results and Discussion

The schematic of an FP interferometer with two infinite silver layers is shown in Figure 1. $L$ represents the distance between the two layers. The thickness of the two layers is represented by $d_1$ and $d_2$. The two layers are arranged perpendicular to the $X$ axis. Incident light propagates along the $X$ axis, and the polarization direction is along the $Z$ axis. Both the discrete dipole approximation method and an analytical model were used for the calculations of the scattering, absorption, and extinction spectra of the interferometer and the electric fields between the two layers. The silver dielectric constants were taken from Palik's book.[51]

The scattering and absorption spectra of an interferometer are shown in Figure 2a. The discrete dipole approximation method with periodic boundary condition was used in the calculations. The grid length in the DDA method was 5 nm. The thickness of the first layer, $d_1$, was 40 nm, and the thickness of the second layer, $d_2$, was 60 nm. Figure 2a shows that a dip in the scattering spectrum is observed at 425 nm wavelength when the distance between the two layers, $L$, was 150 nm. Enhanced absorption at the same wavelength was also obtained. Figure 2b shows the electric field, $|E|^2$, between the two layers at the resonance wavelength of 425 nm. The distance in Figure 2b is measured along the $X$ axis (wave vector direction) from the upper surface of the first layer. Figure 2b indicates that $|E|^2$ between the two layers can be enhanced by a factor of 12 times that of the incident intensity. The highest enhanced electric field is located exactly in the middle of the two layers, which is 75 nm from the surface of each layer.

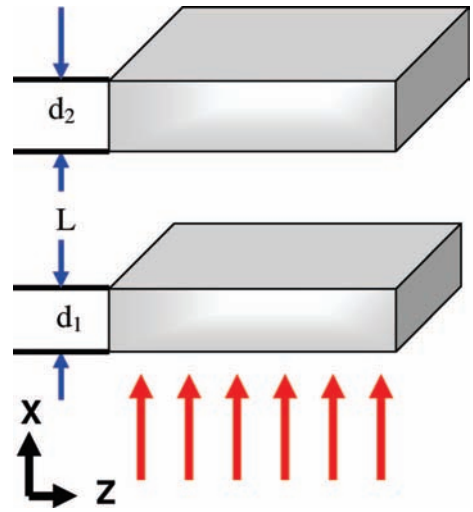


**Figure 1.** Schematic of a Fabry−Pérot interferometer made up of two infinite silver layers. L refers to the distance between the two layers; $d_1$ and $d_2$ represent the thickness of the first and the second layer, respectively.

Before investigating the effect of layer thickness and separation on the spectra and the enhanced electric field between the two layers, we tested the convergence of the DDA program with a 5 nm grid length by comparing the calculated scattering spectra from the DDA program with those obtained from the analytical model. The comparison will validate the reliability of both the DDA program and the analytical model. The numerical DDA method can be applied for applications to other problems that cannot be solved analytically.

The scattering spectra of a two-layer silver film from both the DDA method and the analytical model are shown in Figure 3. The thicknesses of the two silver layers are $d_1 = 40$ nm and $d_2 = 60$ nm. The scattering spectra of the interferometer ($L = 150$ nm) from the DDA program (solid line) and the analytical model (dotted line) are displayed in Figure 3a and demonstrate a good agreement between the DDA program and the analytical model. The scattering spectra for the interferometer for $L = 250$ nm are shown in Figure 3b. The resonance wavelength from the analytical model was 605 nm, which is slightly different from the resonance peak of 609 nm obtained from the DDA program. The 4 nm wavelength difference is due to the large grid length (5 nm) used in the DDA program. When a smaller grid length was used, a good agreement between the two calculations was achieved. A smaller grid length in the DDA program results in a longer computational time. To save computer time, we used the spectra and electric fields calculated from the analytical model in the following discussions.

We calculated the scattering, absorption, and extinction spectra of a two-layer film with 40 ($d_1$) nm and 60 ($d_2$) nm thickness and layer separations ranging from $L = 150$ nm to $L$

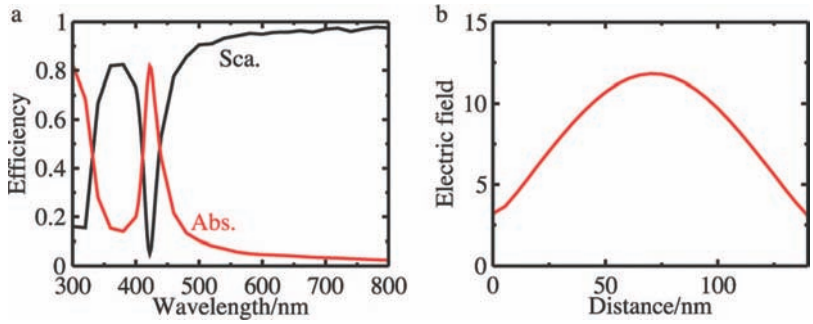


**Figure 2.** (a) Scattering and absorption spectra of an interferometer with two silver layers of 40 ($d_1$) and 60 ($d_2$) nm thickness and $L = 150$ nm. (b) Enhanced electric field, $|E|^2$, between the two layers at the resonance wavelength of 425 nm. The distance was measured along the $X$ axis from the upper surface of the first layer.

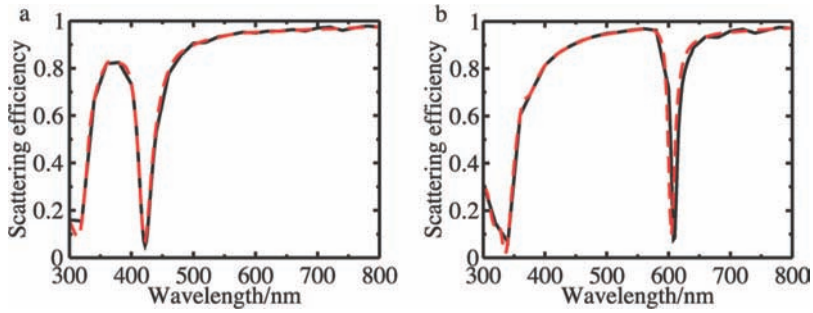


**Figure 3.** Calculated scattering spectra of an interferometer with two silver layers of 40 ($d_1$) and 60 ($d_2$) nm thicknesses and (a) $L = 150$ nm and (b) $L = 250$ nm obtained from both the DDA method (solid line) and the analytical model (dotted line).

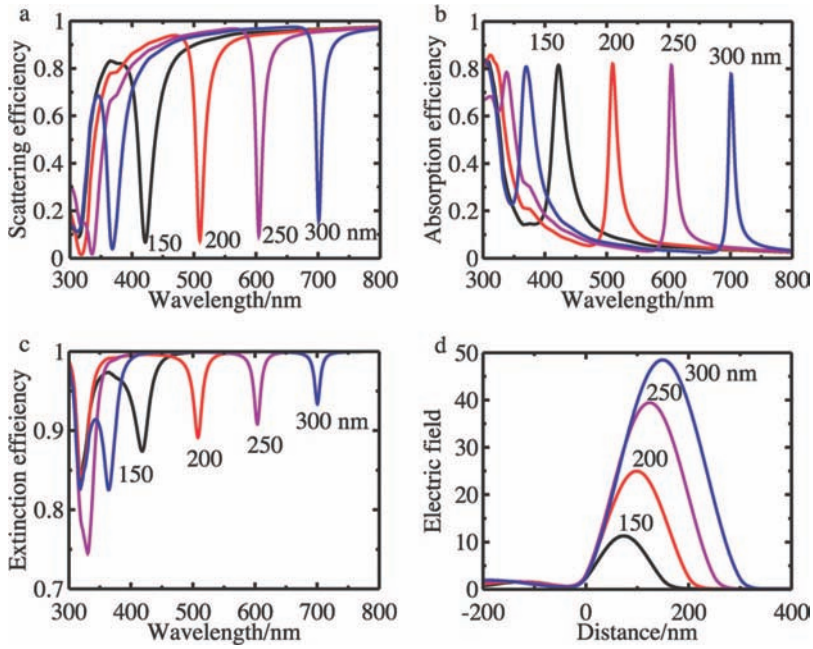


**Figure 4.** (a) Scattering, (b) absorption, and (c) extinction spectra of a two-layer film with 40 ($d_1$) and 60 ($d_2$) nm thicknesses and different separations ($L$) from 150 to 300 nm. (d) $|E|^2$ along the $X$ axis of the film for different values of $L$ at corresponding resonance wavelengths.

= 300 nm. The scattering spectra are shown in Figure 4a and indicate that the resonance wavelength is proportional to the distance between the two layers. The resonance wavelength shifted from 418 to 701 nm when the separation increased from 150 to 300 nm. The ratio of the resonance wavelength change versus the change in layer separation, $d\lambda/dL$, was 1.9 and varied slightly when the thickness of either of the two layers was changed. The resonance width narrowed and the scattering efficiency at resonance wavelength increased with increasing layer separation. This behavior is understandable since the scattering efficiency of a single silver film becomes larger with increasing incident wavelength. The absorption and extinction spectra of the film are shown in Figure 4b and c. The resonance wavelengths for both the absorption and the extinction spectra are the same as those of the scattering spectra. With increasing layer separation, the absorption resonance width narrowed and the intensity of the absorption peak changed slightly. The extinction intensity at the resonance wavelength grew with increasing layer separation, which is consistent with the behavior of the scattering efficiency. We also calculated the electric field, $|E|^2$, along the $X$ axis as shown in Figure 4d. The distances in Figure 4d and the following electric field calculations were

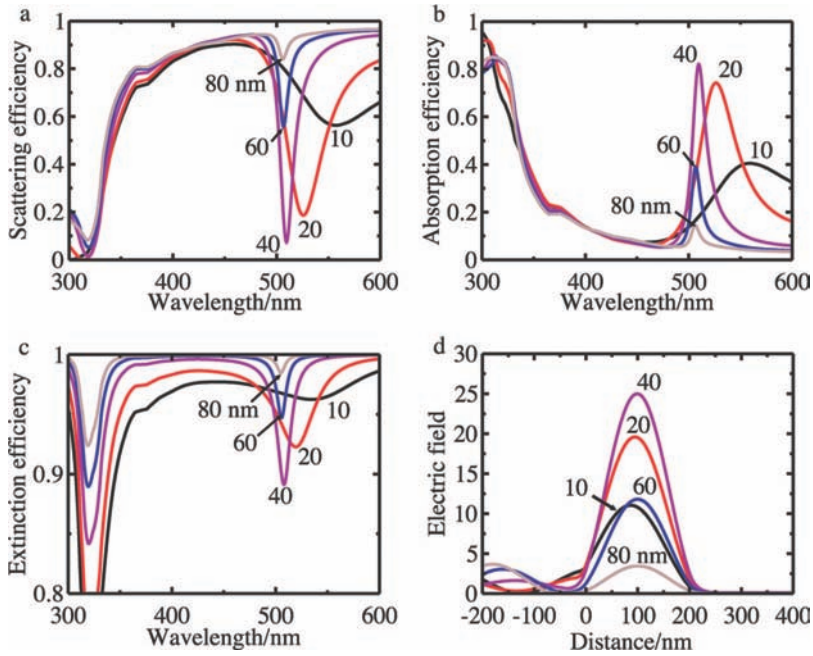


**Figure 5.** (a) Scattering, (b) absorption, and (c) extinction spectra of a two-layer silver film with a fixed separation ($L$) of 200 nm and second layer thickness ($d_2$) of 60 nm. The thickness of the first layer ($d_1$) was changed from 10 to 80 nm. (d) $|E|^2$ along the $X$ axis of the film for different values of $d_1$ at corresponding resonance wavelengths.

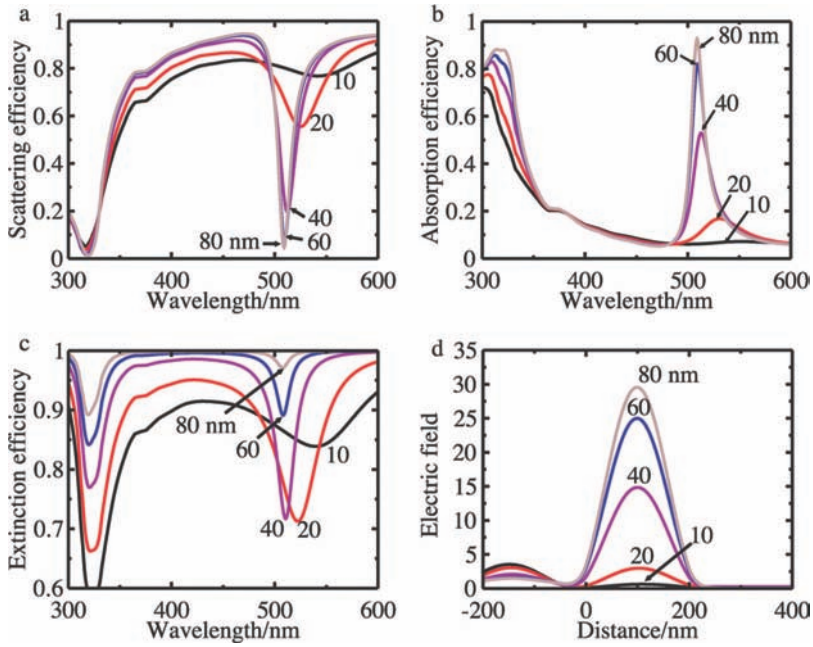


**Figure 6.** (a) Scattering, (b) absorption, and (c) extinction spectra of a two-layer silver film with a fixed separation ($L$) of 200 nm and a first-layer thickness ($d_1$) of 40 nm. The thickness of the second layer ($d_2$) was varied from 10 to 80 nm. (d) $|E|^2$ along the X axis of the film for different values of $d_2$ at corresponding resonance wavelengths.

measured along the $X$ axis from the upper surface of the first layer. Figure 4d shows that the electric field, $|E|^2$, between the two layers was enhanced with the shape of a sine function. The electric field might increase or decrease with the distance from the lower surface of the first layer, depending on the incident wavelength. The electric field became a constant with the same value of transmittance after the second layer. When the distance between the two layers was 150 nm, the enhancement of $|E|^2$ by a factor of 11 could be obtained at a resonance wavelength of 418 nm. The enhancement factor grew to 48 at 701 nm resonance wavelength for $L = 300$ nm. The amplification of the enhancement factor is attributed to the increased reflectivity of the silver layers at longer wavelength. Once incident light penetrates through the first layer, layers with a higher reflectivity will allow multiple reflections of the electromagnetic wave between the two layers and will generate an enhanced electric field between the layers. On the other hand, the increased reflectivity of the first layer will also block the transmission of the incident light. We will show that there is an optimized layer thickness to achieve the highest enhanced electric field between the two layers.

We examined the influence of the layer's thickness ($d_1$) on the spectra of the interferometer and the enhancement factors of electric fields between the two layers. The scattering, absorption, and extinction spectra and the enhanced electric fields of the interferometer are shown in Figure 5. In the

calculations, the thickness of the second layer ($d_2$) was kept at 60 nm, and the distance between the two layers ($L$) was set at 200 nm. $d_1$ was varied from 10 to 80 nm. Figure 5a shows that a broad dip can be observed at the 557 nm wavelength when $d_1 = 10$ nm. The resonance wavelength was shifted to shorter wavelengths, and the resonance width was narrowed when $d_1$ was increased. The resonance peak was blue-shifted to 510 nm wavelength with a decreased scattering efficiency of 0.077 when $d_1$ became 40 nm. Further increasing $d_1$ led to a shorter resonance wavelength and increased scattering efficiency at resonance wavelength. When $d_1$ was increased to 80 nm, the resonance scattering efficiency at 506 nm wavelength grew to 0.84.

The absorption spectra in Figure 5b displayed the same blue shift when $d_1$ was increased from 10 to 80 nm. The intensity of the resonance absorption increased when $d_1$ was increased from 10 to 40 nm and dropped dramatically when $d_1$ was further increased to 80 nm. The change of the absorption spectra was consistent with that of the scattering spectra. A reduced scattering led to enhanced absorption. The extinction spectra of the films are shown in Figure 5c. Figure 5c indicates that the extinction efficiencies at nonresonance wavelength increase proportionally with the thickness of the first layer. Near resonance wavelength, when $d_1$ was increased from 10 to 40 nm, the resonance extinction efficiency decreased from 0.96 at 524 nm wavelength to 0.89 at 508 nm wavelength. The smaller extinction efficiency was attributed to a stronger Fabry−Pérot effect when $d_1$ was increased from 10 to 40 nm. When $d_1$ was further increased, the extinction efficiency increased due to a significant increase in the reflectivity of the first layer. The resonance width always narrowed with increasing $d_1$, which was consistent with Zou's previous work about the layer thickness dependence of the extinction spectra for a spherical silver core shell particle.[52] Figure 5d displays the enhanced electric field of the interferometer. The electric field enhancement factor is proportional to the absorption efficiency with the strongest absorption efficiency leading to the highest enhanced electric field between the two layers. Figure 5d shows that $|E|^2$ was enhanced by a factor of 11 when $d_1$ was 10 nm. The enhancement factor grew to 25 when $d_1$ was changed to 40 nm and dropped to 3.5 when $d_1$ was further increased to 80 nm. We also notice that the distance of the highest electric field from the first layer surface increased from 86 to 100 nm (half the separation distance between the two layers) when $d_1$ was varied from 10 to 80 nm.

We investigated the influence of the second layer thickness ($d_2$) on the spectra of the film and on the enhanced electric fields between the two layers. The scattering, absorption, and extinction spectra and the electric field distribution along the $X$ axis are shown in Figure 6. Figure 6a shows that the scattering efficiency of the interferometer at nonresonance wavelength grows with increasing $d_2$. At resonance wavelength, the scattering efficiency monotonically decreased with increasing $d_2$. The resonance width narrowed and the resonance wavelength blue-shifted with increasing $d_2$, which exhibits the same trend as $d_1$. The absorption resonance wavelength as shown in Figure 6b also shifted to blue and resonance width narrowed with increasing $d_2$. The absorption intensity monotonically grew with increase $d_2$. The influence of $d_2$ on the extinction spectra, which is shown in Figure 6c, is similar to that of $d_1$. The lowest resonance extinction efficiency was observed when $d_2$ was 20 nm. The enhanced electric fields between the two layers are shown in Figure 6d. Figure 6d indicates that the enhanced electric field becomes stronger with increasing $d_2$. The electric field between the two layers is 0.61 when $d_2 = 10$ nm. The enhancement grew to 30 when $d_2$ was changed to 80 nm. The distance of the highest electric field from the first layer surface was varied from 107 to 100 nm when $d_2$ grew from 10 to 80 nm.

We also examined the optical properties of interferometer with other configurations and found that the lowest scattering efficiency and the highest absorption efficiency of the interferometer could be observed when the thickness of the first layer ($d_1$) was about 30 nm and the thickness of the second layer ($d_2$) was greater than 80 nm. The highest enhanced electric field between the two layers was also obtained at the same conditions.

## Conclusion

We studied the scattering, absorption, and extinction spectra and the enhanced electric field of a two-layer silver film with different thicknesses and separations. The resonance wavelength shifted to red with increasing layer separations. Both the first and the second layer thickness significantly influenced the optical properties of the film. Reduced scattering and enhanced absorption could be obtained when the thickness of the second layer was larger than 80 nm and the thickness of the first layer was about 30 nm. An enhancement of the electric field, $|E|^2$, of 50 was demonstrated between the two layers at 701 nm resonance wavelength when $d_1 = 40$ nm, $d_2 = 60$, and $L = 300$ nm.

**Acknowledgment.** This work was supported by the ACS Petroleum Research Fund No. 48268-G6 and NSF CBET 0827725 Fund.

## References and Notes

(1) Hernandez G. *Fabry−Perot Interferometers (Cambridge Studies in Modern Optics)*; Cambridge University Press: Cambridge, 1986.
(2) Li, C. H.; Benedick, A. J.; Fendel, P.; Glenday, A. G.; Kaertner, F. X.; Phillips, D. F.; Sasselov, D.; Szentgyorgyi, A.; Walsworth, R. L. *Nature* **2008**, *452*, 610.
(3) Srinivasan, K.; Painter, O. *Nature* **2007**, *450*, 862.
(4) Lin, V. S.; Motesharei, K.; Dancil, K. P.; Sailor, M. J.; Ghadiri, M. R. *Science* **1997**, *278*, 840.
(5) Lu, G.; Cheng, B.; Shen, H.; Zhou, Y.; Chen, Z.; Yang, G.; Tillement, O.; Roux, S.; Perriat, P. *Appl. Phys. Lett.* **2006**, *89*, 223904.
(6) Song, W. Z.; Zhang, X. M.; Liu, A. Q.; Lim, C. S.; Yap, P. H.; Hosseini, H. M. M. *Appl. Phys. Lett.* **2006**, *89*, 203901.
(7) Lu, T.; Li, Z.; Du, Q.; Bi, J. *Sens. Actuators, A* **2008**, *148*, 83.
(8) Machavaram, V. R.; Badcock, R. A.; Fernando, G. F. *Sens. Actuators, A* **2007**, *138*, 248.
(9) Liang, W.; Bockrath, M.; Bozovic, D.; Hafner, J. H.; Tinkham, M.; Park, H. *Nature* **2001**, *411*, 665.
(10) Zhang, Y.; Huang, W.; Li, B. *Appl. Phys. Lett.* **2008**, *93*, 031110.
(11) Schartner, S.; Austerer, M.; Schrenk, W.; Andrews, A. M.; Klang, P.; Strasser, G. *Opt. Express* **2008**, *16*, 11920.
(12) Pruessner, M. W.; Stievater, T. H.; Rabinovich, W. S. *Opt. Lett.* **2007**, *32*, 533.
(13) Yoshida, H.; Yamashita, Y.; Kuwabara, M.; Kan, H. *Nat. Photonics* **2008**, *2*, 551.
(14) Yu, N.; Fan, J.; Wang, Q.; Pflügl, C.; Diehl, L.; Edamura, T.; Yamanishi, M.; Kan, H.; Capasso, F. *Nat. Nanotechnol.* **2008**, *2*, 564.
(15) Zheludev, N. I.; Prosvirnin, S. L.; Papasimakis, N.; Fedotov, V. A. *Nat. Photonics* **2008**, *2*, 351.
(16) Stockman, M. I. *Nat. Photonics* **2008**, *2*, 327.
(17) Manolatou, C.; Rana, F. *IEEE J. Quantum Electron.* **2008**, *44*, 435.
(18) Zimmler, M. A.; Bao, J.; Capasso, F.; Müller, S.; Ronning, C. *Appl. Phys. Lett.* **2008**, *93*, 051101.
(19) Weitz, D. A.; Garoff, S.; Gersten, J. I.; Nitzan, A. *J. Chem. Phys.* **1983**, *78*, 5324.
(20) Benner, R. E.; Barber, P. W.; Owen, J. F.; Chang, R. K. *Phys. Rev. Lett.* **1980**, *44*, 475.
(21) Tam, F.; Goodrich, G. P.; Johnson, B. R.; Halas, N. J. *Nano Lett.* **2007**, *7*, 496.
(22) Pompa, P. P.; Martiradonna, L.; Della Torre, A.; Della Sala, F.; Manna, L.; De Vittorio, M.; Calabi, F.; Cingolani, R.; Rinaldi, R. *Nat. Nanotechnol.* **2006**, *1*, 126.

(23) Zhang, G.; Malicka, J.; Gryczynski, I.; Lakowicz, J. R. *J. Phys. Chem. B* **2006**, *109*, 9499.
(24) Ray, K.; Badugu, R.; Lakowicz, J. R. *J. Am. Chem. Soc.* **2006**, *128*, 8998.
(25) Johansson, P.; Xu, H.; Kall, M. *Phys. Rev. B* **2005**, *72*, 035427.
(26) Lee, J.; Govorov, A. O.; Dulka, J.; Kotov, N. A. *Nano Lett.* **2004**, *4*, 2323.
(27) Cohanoschi, I.; Thibert, A.; Toro, C.; Zou, S.; Hernandez, F. E. *Plasmonics* **2007**, *2*, 89.
(28) Biteen, J. S.; Sweatlock, L. A.; Mertens, H.; Lewis, N. S.; Polman, A.; Atwater, H. A. *J. Phys. Chem. C* **2007**, *111*, 13372.
(29) Bergman, D. J.; Stockman, M. I. *Phys. Rev. Lett.* **2003**, *90*, 027402.
(30) Lal, S.; Grady, N. K.; Goodrich, G. P.; Halas, N. J. *Nano Lett.* **2006**, *6*, 2338.
(31) Zou, S.; Schatz, G. C. *Chem. Phys. Lett.* **2004**, *403*, 62.
(32) Qin, L.; Zou, S.; Xue, C.; Atkison, A.; Schatz, G. C.; Mirkin, C. A. *Proc. Natl. Acad. Sci. U.S.A.* **2006**, *103*, 13300.
(33) Kneipp, K.; Wang, Y.; Kneipp, H.; Perelman, L. T.; Etzkan, I.; Dasari, R. R.; Feld, M. S. *Phys. Rev. Lett.* **1977**, *78*, 1667.
(34) Jeanmaire, D. L.; Van Duyne, R. P. *J. Electroanal. Chem.* **1977**, *84*, 1.
(35) Cao, Y. W. C.; Jin, R. C.; Mirkin, C. A. *Science* **2002**, *297*, 1536.
(36) Xu, H.; Bjerneld, E. J.; Kall, M.; Borjesson, L. *Phys. Rev. Lett.* **1999**, *83*, 4357.
(37) Nie, S.; Emory, S. R. *Science* **1997**, *275*, 1102.
(38) Michaels, A. M.; Jiang, J.; Brus, L. *J. Phys. Chem. B* **2000**, *104*, 11965.
(39) Orendorff, C. J.; Gole, A.; Sau, T. K.; Murphy, C. *J. Anal. Chem.* **2005**, *77*, 3261.
(40) Tovmachenko, O. G.; Graf, C.; van den Heuvel, D. J.; van Blaaderen, A.; Gerritsen, H. C. *Adv. Mater.* **2006**, *18*, 91.
(41) Pons, T.; Medintz, I. L.; Sapsford, K. E.; Higashiya, S.; Grimes, A. F.; English, D. S.; Mattoussi, H. *Nano Lett.* **2007**, *7*, 3157.
(42) Nikoobakht, B.; Burda, C.; Braun, M.; Hun, M.; El-Sayed, M. A. *Photochem. Photobiol.* **2002**, *75*, 591.
(43) Gueroui, Z.; Libchaber, A. *Phys. Rev. Lett.* **2004**, *93*, 166108.
(44) Kim, Y. P.; Oh, Y. H.; Oh, E.; Ko, S. H.; Han, M. K.; Kim, H. S. *Anal. Chem.* **2008**, *80*, 4634.
(45) Gadenne, B.; Yildiz, I.; Amelia, M.; Ciesa, F.; Secchi, A.; Arduini, A.; Credi, A.; Raymo, F. M. *J. Mater. Chem.* **2008**, *18*, 2022.
(46) Zhang, J.; Badugu, R.; Lakowicz, J. R. *Plasmonics* **2008**, *3*, 3.
(47) Draine, B. T.; Flatau, P. J. *User Guide for the Discrete Dipole Approximation Code DDSCAT.7.0*; 2008; http://arxiv.org/abs/0808.0337.
(48) Zou, S.; Schatz, G. C. *J. Chem. Phys.* **2004**, *121*, 12606.
(49) Bohren, C. F.; Huffman, D. R. *Absorption and Scattering of Light by Small Particles*; Wiley: New York, 1983.
(50) P, Y. *Optical Waves in Layered Media*; Wiley: New York, 1988.
(51) Palik, E. D. *Handbook of Optical Constants of Solids*; Academic Press: New York, 1985.
(52) Zou, S. *Chem. Phys. Lett.* **2008**, *454*, 289.

JP810756E